THE AMERICAN SOCIETY OF MECHANICAL ENGINEERS
345 E. 47 St., New York, N.Y. 10017

86-G

Three-Dimensional Flowfield Calculation of High-Loaded Centrifugal Compressor Diffusers

INGOLF TEIPEL
ALEXANDER WIEDERMANN
Institute of Mechanics
University of Hannover
Germany

In this paper a method for calculating inviscid three-dimensional flowfields in vaned diffusers of high-loaded centrifugal compressors will be considered. Following the classical theory of Wu different kinds of stream surfaces have been introduced. The complete three-dimensional result is approximated by a combination of blade to blade stream surfaces (S_1-surface) and S_2-surfaces between the side walls of the diffuser. The geometry of the stream sheets depends on each other. A special curvilinear coordinate system has been introduced to take into account the twisted shape of the surfaces.

Because of the expected transonic flow pattern due to the high loading of the considered units a time marching procedure is applied for solving the conservative form of the governing equations in each kind of the stream surfaces.

To demonstrate the capability of the described calculation procedure the flow pattern in a radial diffuser with twisted vanes has been considered. The impeller speed is assumed to be so large that the flow may become transonic behind the impeller exit. Shock waves may therefore occur in front of the diffuser vanes. Pressure distributions have been calculated in several stream sheets and have been compared with available experimental data. Also integral results predicted by this theory have been compared with measured performance maps. A simple method to estimate a diffuser blockage factor will be given. As a conclusion it will be indicated that a good agreement between theory and experiment justifies the application of an inviscid three-dimensional method for calculating essential details of the pressure field in radial diffusers. However, a coupling of inviscid theory and boundary layer theory does not provide a sufficient prediction of the losses.

NOMENCLATURE

b	diffuser width,m
c_p	pressure recovery coefficient
e	specific energy, J/kg
$\vec{F}$	vector, def. in eqs. (1) and (4)
$\vec{G}$	vector, def. in eqs. (1) and (4)
$\vec{F}^*$	vector, def. in eqs. (1) and (4)
$\vec{G}^*$	vector, def. in eqs. (1) and (4)
h	specific enthalpy, J/kg
h_t	total enthalpy, J/kg
$\dot{m}_D$	dimensionless mass flux, def. in eq. (9)
$\underline{M}_1$	diagonal matrix, def. in eqs. (1) and (4)
$\underline{M}_2$	diagonal matrix, def. in eqs. (1) and (4)
$\underline{M}_3$	diagonal matrix, def. in eqs. (1) and (4)
n_{red}	rotational speed, red. to norm condition
$\vec{P}$	vector, def. in eqs. (1) and (4)
p	pressure, bar
p_t	total pressure, bar
r	radius, m
S	function of the S_1-stream surface
t	time, s
$\vec{U}$	vector, def. in eqs. (1) and (4)
$\vec{u}$	velocity vector, m/s
u_x	x-component of velocity, m/s
u_y	y-component of velocity, m/s
u_r	radial velocity component, m/s
u_θ	tangential velocity component, m/s
u_z	axial velocity component, m/s
z	axial coordinate, m
γ	ratio of specific heats
Φ	function of the S_2-stream surface
Θ	angle
λ	diffuser radius ratio, $\lambda = r/r_{IE}$
λ,ν	angles of the S_1-stream sheet, rad
μ,ω	angles of the S_2-stream sheet, rad
π	= 3.1415...
ϱ	density, kg/m^3

Presented at the International Gas Turbine Conference and Exhibit
Dusseldorf, West Germany—June 8-12, 1986

ϱ_t	total density, kg/m^3
σ	thickness of the S_1-stream sheet, m
τ	angle, proportional to the thickness of the S_2-stream sheet, rad

INDICES

IE	Impeller exit
DE	Diffuser exit
S_1	S_1-stream sheet
S_2	S_2-stream sheet

INTRODUCTION

High stage efficiency and loading are desired properties of today's centrifugal compressor units. They can be achieved by increasing the rotational speed of the impeller. As a consequence the kinetic energy at the impeller exit will become so large that vaneless diffusers will no longer be suited for an efficient pressure recovery [1]. Therefore compressors have to be equipped with vaned diffusers. The blades might be formed with respect to aerodynamic rules [2].

Due to a very strong interaction between the impeller and diffuser there are several facts to be taken into account for designing the diffuser vanes. Firstly supersonic regions including shock waves might occur in front of the blades. The requirements for calculating transonic flowfields can be completed by introducing a time marching procedure as has been done by Jeske and Teipel [3]. Secondly the appearance of secondary flow motion in the impeller passages produces an energy gradient from hub to tip which leads to a variation of the flow angle between the diffuser side walls at the impeller exit as shown by measurements performed by Jansen [4]. In order to fit the geometry of the blades to the varying stream directions Jansen designed a three-dimensionally twisted blade passage shown in Fig. 1. As can be seen the value of the blade angle at the leading edge reaches from nearly 0 to 33 degrees. In order to calculate the three dimensional flow pattern Wiedermann [5] recently applied a quasi-three-dimensional method based on a general theory first given by Wu [6].

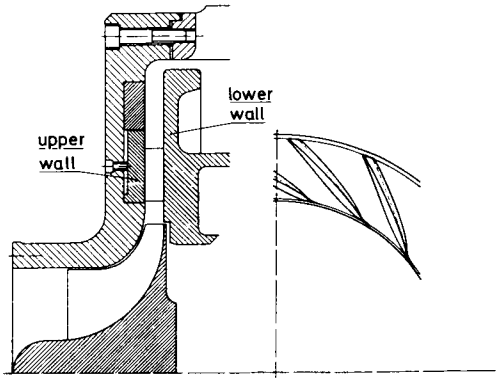

FIG. 1 Design of the twisted diffuser (Jansen [4])

DESCRIPTION OF THE METHOD

Although modern vector computers like the CRAY 1 or CYBER 205 become available for more and more research laboratories the calculation of complete three-dimensional flowfields with complex boundaries has remained a time consuming process. Therefore several attempts for an approximate solution procedure of the flowfield has been made. One of the most common approaches was published by Wu in 1952 [6]. Wu suggested to describe the complete three-dimensional flow as a number of two-dimensional flowfields. He introduced S_1-stream surfaces (blade-to-blade surfaces) and S_2-stream sheets between the side walls. The location of the different stream sheets in a centrifugal diffuser passage is illustrated in Fig. 2. As the geometry of the different kinds of stream surfaces depends on each other one obtains an approximate solution of the three-dimensional flowfield. Matrix methods [6,7,8] as well as streamline curvature methods [9,10] have been developed for solving the governing equations in each kind of the stream surfaces. Krimerman and Adler [11] as well as Hirsch [12] were, at least, the first who succeeded in applying the complete theory of Wu. Hirsch replaced the flow along the S_2-surfaces by the calculation of the exact mass averaged - pitch averaged flow in a meridional plane whereas Krimerman and Adler used several twisted S_2 - stream surfaces, the shapes of which had been determined by the results in various S_1-stream sheets. They calculated the flowfield in a centrifugal impeller using a finite element procedure. Recently also Wang et al. [13] published a complete quasi-three-dimensional method for predicting subsonic flowfields.

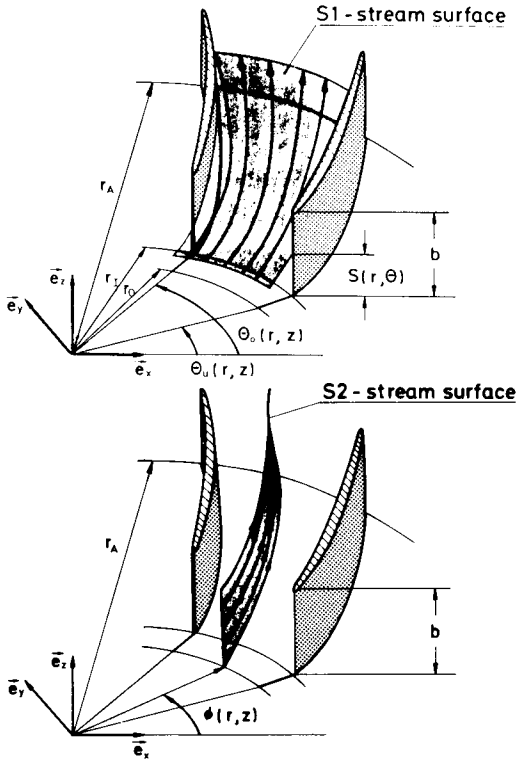

FIG. 2 S_1- and S_2-stream surfaces in a centrifugal compressor diffuser

In the present method the application of Wu's theory has been preferred to a complete three-dimensional approach because it was the authors' purpose to avoid large computer storage and CP - time requirements. The results obtained in three S_1- and three S_2-stream surfaces have been coupled to build up an approximate solution of the three-dimensional flowfield in Jansen's twisted diffuser channel. The stream sheets are arranged as shown in Fig. 2. The structure of the complete calculation procedure is demonstrated in Fig. 3. At first the pressure fields in plane blade-to-blade surfaces at different axial locations will be calculated. Then the shapes of the three S_2-stream sheets are given by the streamlines obtained in each S_1-stream surface. In general they are twisted in a complicated manner. The last step of a convergence cycle is the calculation of the flowfields in the corrected S_1-stream sheets. Theoretically the loop can be repeated until a sufficient convergence limit is reached; but due to immense CPU-times at a conventional CDC-CYBER 76 the calculation procedure has been stopped after the S_1-stream surfaces had been improved once.

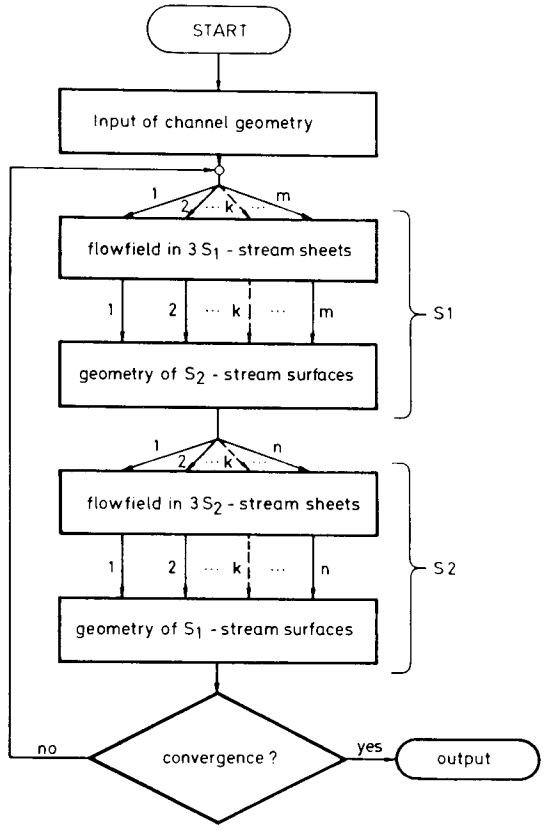

FIG. 3 Computational scheme of the applied quasi-three-dimensional procedure

THE GOVERNING EQUATIONS

In order to calculate transonic flowfields which include shock waves a conservative formulation of the governing equations is desireable. Due to the complicated twisted shape of the stream sheets the equations contain a large amount of geometrical parameters.

Using cylinder coordinates the governing equations for calculating flowfields in S_1-stream sheets can be written in a conservative form:

$$\frac{\partial \vec{U}_{S_1}}{\partial t} + \frac{\partial \vec{F}_{S_1}}{\partial r} + \frac{\partial \vec{G}_{S_1}}{\partial \Theta} + \underline{M}_1 \left[\frac{\partial \vec{F}^*_{S_1}}{\partial r} + \frac{\partial \vec{G}^*_{S_1}}{\partial \Theta} \right] + \underline{M}_2 \frac{\partial \vec{P}_{S_1}}{\partial r} + \underline{M}_3 \frac{\partial \vec{P}_{S_1}}{\partial \Theta} = \vec{0} \qquad (1)$$

with the matrices

$$\vec{U}_{S_1} = \begin{bmatrix} r\sigma\varrho \\ r\sigma\varrho \left[u_x + u_z (\tan\lambda \cos\Theta - \tan\nu \sin\Theta) \right] \\ r\sigma\varrho \left[u_y + u_z (\tan\lambda \sin\Theta + \tan\nu \cos\Theta) \right] \\ r\sigma\varrho \left[e + \frac{1}{2} \vec{u} \cdot \vec{u} \right] \end{bmatrix}$$

$$\vec{F}_{S_1} = \begin{bmatrix} r\sigma\varrho u_r \\ r\sigma\varrho u_x u_r \\ r\sigma\varrho u_y u_r \\ r\sigma\varrho u_r \left[h + \frac{1}{2} \vec{u} \cdot \vec{u} \right] \end{bmatrix} \quad \vec{G}_{S_1} = \begin{bmatrix} \sigma\varrho u_\Theta \\ \sigma\varrho u_x u_\Theta \\ \sigma\varrho u_y u_\Theta \\ \sigma\varrho u_\Theta \left[h + \frac{1}{2} \vec{u} \cdot \vec{u} \right] \end{bmatrix}$$

$$\vec{F}^*_{S_1} = \begin{bmatrix} 0 \\ r\sigma\varrho u_z u_r \\ r\sigma\varrho u_z u_r \\ 0 \end{bmatrix} \quad \vec{G}^*_{S_1} = \begin{bmatrix} 0 \\ \sigma\varrho u_z u_\Theta \\ \sigma\varrho u_z u_\Theta \\ 0 \end{bmatrix} \quad \vec{P}_{S_1} = \begin{bmatrix} 0 \\ p \\ p \\ 0 \end{bmatrix}$$

$$\underline{M}_1 = \begin{bmatrix} 0 & 0 & 0 & 0 \\ 0 & \tan\lambda\cos\Theta - \tan\nu\sin\Theta & 0 & 0 \\ 0 & 0 & \tan\lambda\sin\Theta + \tan\nu\cos\Theta & 0 \\ 0 & 0 & 0 & 0 \end{bmatrix}$$

$$\underline{M}_2 = r\sigma \begin{bmatrix} 0 & 0 & 0 & 0 \\ 0 & \cos\Theta & 0 & 0 \\ 0 & 0 & \sin\Theta & 0 \\ 0 & 0 & 0 & 0 \end{bmatrix} \qquad (2)$$

$$\underline{M}_3 = \sigma \begin{bmatrix} 0 & 0 & 0 & 0 \\ 0 & -\sin\Theta & 0 & 0 \\ 0 & 0 & \cos\Theta & 0 \\ 0 & 0 & 0 & 0 \end{bmatrix}$$

The angles λ and ν are given by

$$\lambda = \arctan\left(\frac{\partial S}{\partial r}\right)$$
$$\nu = \arctan\left(\frac{1}{r}\frac{\partial S}{\partial \Theta}\right) \qquad (3)$$

where $z = S(r,\Theta)$ means the function of the S_1-stream surface. σ is a factor which is proportional to the axial stream sheet thickness. As the S_1-surfaces are only slightly curved the angles λ and ν can be neglected.

For the S_2-stream surfaces, which are strongly twisted in general, the conservative form of the governing equations yields

$$\frac{\partial \vec{U}_{S_2}}{\partial t} + \frac{\partial \vec{F}_{S_2}}{\partial r} + \frac{\partial \vec{G}_{S_2}}{\partial z} + \underline{M}_1\left[\frac{\partial \vec{F}^*_{S_2}}{\partial r} + \frac{\partial \vec{G}^*_{S_2}}{\partial z}\right] + \underline{M}_2\frac{\partial \vec{P}_{S_2}}{\partial r} + \underline{M}_3\frac{\partial \vec{P}_{S_2}}{\partial z} = \vec{0} \qquad (4)$$

with the matrices

$$\vec{U}_{S_2} = \begin{bmatrix} r\tau\varrho \\ r\tau\varrho\,(u_x + \tan(\mu+\Phi)\,u_y) \\ r\tau\varrho\,(u_z + \frac{\tan\omega}{\cos\Phi - \sin\Phi\tan\mu}\,u_y) \\ r\tau\varrho\left[e + \frac{1}{2}\vec{u}\cdot\vec{u}\right] \end{bmatrix}$$

$$\vec{F}_{S_2} = \begin{bmatrix} r\tau\varrho u_r \\ r\tau\varrho u_x u_r \\ r\tau\varrho u_z u_r \\ r\tau\varrho u_r\left[h + \frac{1}{2}\vec{u}\cdot\vec{u}\right] \end{bmatrix} \quad \vec{G}_{S_2} = \begin{bmatrix} r\tau\varrho u_z \\ r\tau\varrho u_x u_z \\ r\tau\varrho u_z^2 \\ r\tau\varrho u_z\left[h + \frac{1}{2}\vec{u}\cdot\vec{u}\right] \end{bmatrix}$$

$$\vec{F}^*_{S_2} = \begin{bmatrix} 0 \\ r\tau\varrho u_y u_r \\ r\tau\varrho u_y u_r \\ 0 \end{bmatrix} \quad \vec{G}^*_{S_2} = \begin{bmatrix} 0 \\ r\tau\varrho u_y u_z \\ r\tau\varrho u_y u_z \\ 0 \end{bmatrix} \quad \vec{P}_{S_2} = \begin{bmatrix} 0 \\ p \\ p \\ 0 \end{bmatrix}$$

$$\underline{M}_3 = \begin{bmatrix} 0 & 0 & 0 & 0 \\ 0 & 0 & 0 & 0 \\ 0 & 0 & r\tau & 0 \\ 0 & 0 & 0 & 0 \end{bmatrix} \qquad (5)$$

$$\underline{M}_1 = \begin{bmatrix} 0 & 0 & 0 & 0 \\ 0 & \tan(\mu+\Phi) & 0 & 0 \\ 0 & 0 & \frac{\tan\omega}{\cos\Phi - \sin\Phi\tan\mu} & 0 \\ 0 & 0 & 0 & 0 \end{bmatrix}$$

$$\underline{M}_2 = r\tau\begin{bmatrix} 0 & 0 & 0 & 0 \\ 0 & \frac{\cos\Phi +}{+\sin\Phi\tan(\mu+\Phi)} & 0 & 0 \\ 0 & 0 & \frac{\tan\omega}{\cot\Phi - \tan\mu} & 0 \\ 0 & 0 & 0 & 0 \end{bmatrix}$$

μ and ω are angles describing the curvature of the stream sheet and being given as derivatives of the stream surface function $\Theta = \Phi(r,z)$ by

$$\mu = \arctan\left(r\frac{\partial \Phi}{\partial r}\right)$$
$$\omega = \arctan\left(r\frac{\partial \Phi}{\partial z}\right) \qquad (6)$$

The angle τ is proportional to the angular thickness of the S_2-stream sheet.

The different rows of the matrices denote the continuity equation, the two remaining independent components of the momentum equation in the considered surface kind and the energy equation. Assuming isoenergetic flow condition the fourth row of the eqs. (1) and (4) can be replaced by an algebraic energy relation. For an ideal gas one gets

$$h_t = \frac{\gamma}{\gamma - 1}\frac{p_t}{\varrho_t} = \frac{\gamma}{\gamma - 1}\frac{p}{\varrho} + \frac{\vec{u}\cdot\vec{u}}{2} \qquad (7)$$

The solutions of the eqs. (1) and (4) are obtained by applying an explicit MacCormack scheme in its original version published in 1969 [13]. To fulfil the boundary conditions a body-fitted coordinate system is introduced. At the solid walls the flowfield variables are calculated in a special coordinate system. At the inlet and outlet section of the computational domain characteristic relations are applied. Further details are outlined in [5].

The modelling of the complicated fluid flow pattern at the impeller exit has to be considered very carefully because of its important influence on the flowfield in the vaneless region of the diffuser. As only the steady state solution is of interest the time-dependent jet-wake structure has not been taken into account. However, the gradient of the total pressure between the diffuser side walls due to secondary flow motion in the impeller passage can be simulated by prescribing a function for p_t which has been derived from experiment. As a consequence the distribution of the flow variables is not uniform in circumferential as well as in axial direction.

COMPARISON OF PREDICTED AND MEASURED FLOWFIELDS

Now the range of application of the described method will be proved by comparing theory with experimental data. The measurements were carried out at the Institute of Turbomachinery at the University of Hannover and reported in [4] and [15].

Measured pressure fields obtained at an impeller rotational speed of 18,000 r.p.m. near the upper and the lower side wall are shown in Figs. 4 and 5. The considered operating point is located nearby the surge line. The graphs contain domains of constant pressure which are related to the maximum total pressure at the impeller exit. The average absolute Mach number at the impeller outlet was about 1.25. The measured isobars indicate a strong pressure rise in the vaneless and semi-vaned region in front of the throat of the diffuser channel while the pressure recovery is only small further downstream. Especially there is a strong pressure gradient at the suction side near the leading edge at the upper side wall (Fig. 4) where high loading at the blades occures. The predicted isobar contours (Figs. 6 and 7) calculated along the corrected stream sheets after one convergence cycle as shown in Fig. 3 correspond well with the measured pattern. Especially the curved shape of the isobars in the vaneless region is in a very close agreement with experiment. As indicated by measurements the essential part

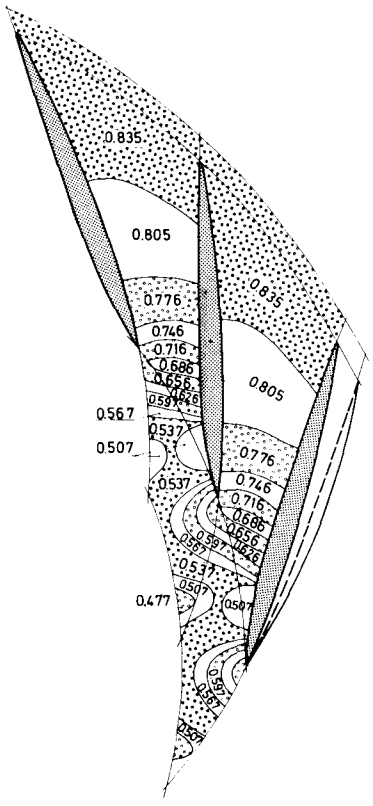

FIG. 4 Regions of constant pressure p/p_t at the upper side wall
Measurements by Jansen et al.[4,15]
n_{red} = 18,000 r.p.m.

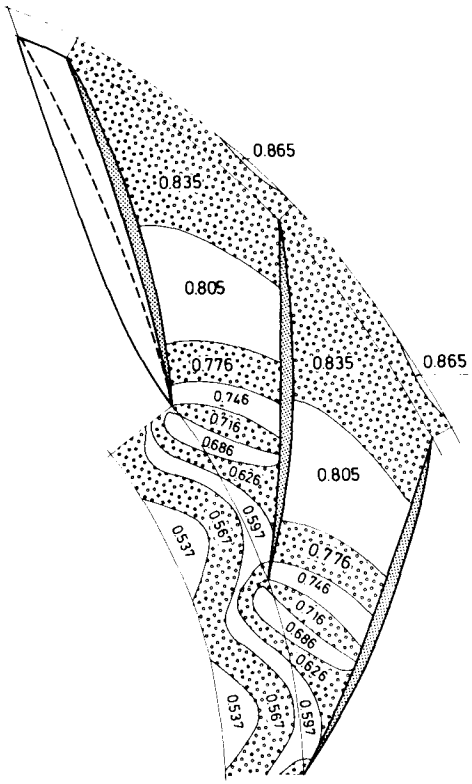

FIG. 5 Regions of constant pressure p/p_t at the lower side wall
Measurements by Jansen et al.[4,15]
n_{red} = 18,000 r.p.m.

of the pressure recovery is predicted to take place in front of the throat. At the lower side wall the wavy contour of pressure lines is well predicted by theory. However, the calculated isobars cumulate strongly in front of the blades while there is no shock observed by experiment. Nevertheless, essential details of the flowfield can be given by applying the present inviscid theory.

In Fig. 8 the isobars in the projection of the three S_2-stream surfaces into the meridional plane have been plotted. As in the S_1-surface nearly all the predicted pressure rise occurs in the vaneless region between λ = 1. and λ = 1.15. The cumulation of the isobars in front of the vanes coincides well with both the predicted data in the S_1-sheets and experiment. Due to the energy gradient at the impeller exit there is a rise of static pressure from lower to upper wall, where the energy is lowest.

A further advantage of the present method is the fact that also velocity and isobar profiles in a θ,z - plane can be constructed by combining several stream sheet solutions. A comparison of measured and predicted flow pattern is given in the next four pictures, Figs. 9 to 12. If an impeller rotational speed of 14,600 r.p.m. is chosen the measured distribution of the absolute flow angle will provide a strong gradient from the lower (z/b = 1) to the upper wall (z/b = 0).

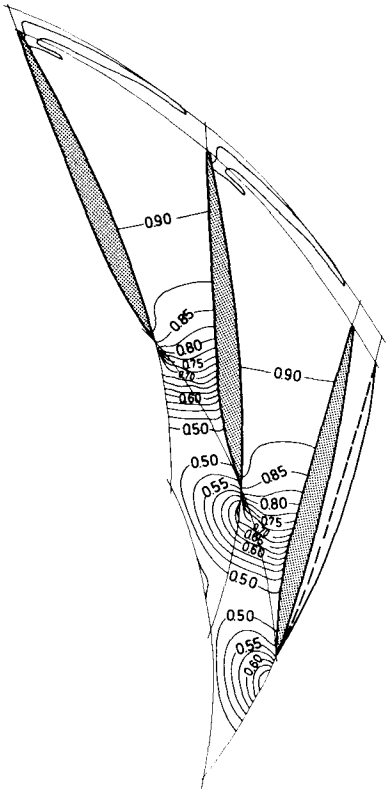

FIG. 6 Calculated isobars p/p_t at the upper side wall n_{red} = 18,000 r.p.m.

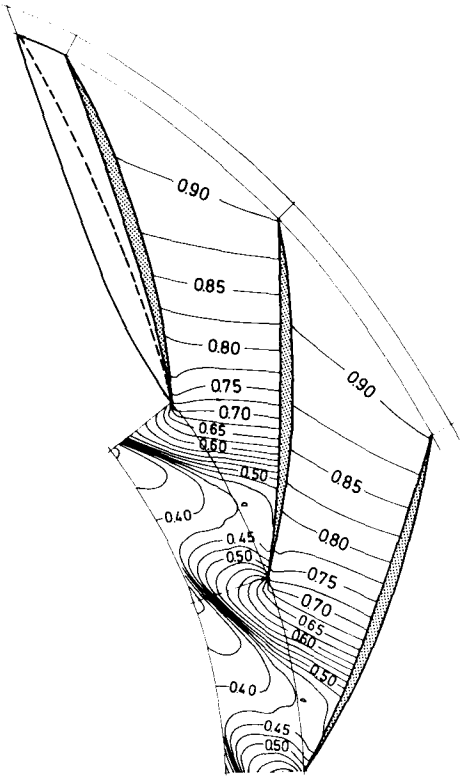

FIG. 7 Calculated isobars p/p_t at the lower side wall n_{red} = 18,000 r.p.m.

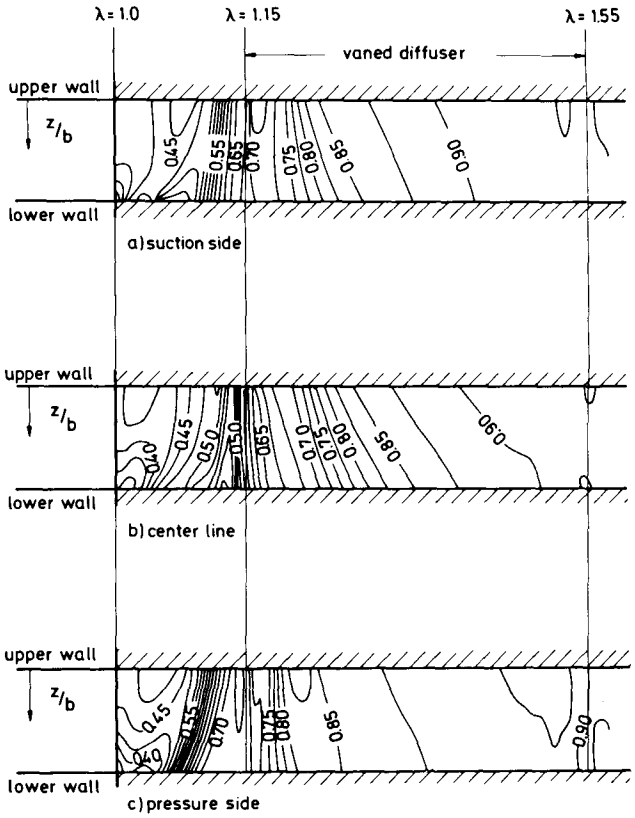

FIG. 8 Calculated isobars p/p_t in the S_2-stream surfaces projected into the meridional plane

After having introduced a variation of the total pressure at the impeller exit from the experiment as one boundary condition at the entrance one gets a close agreement between measured and predicted profiles. However, the very small numbers of the flow angle near the upper wall cannot be calculated satisfactorily by the present theory because of the absence of any friction terms.

Also the comparison of predicted and measured Mach line contours in front of the vaned diffuser offers a reasonably good agreement as shown in Figs. 11 and 12. It is noticeable that especially the location of the maximum and the minimum of the profile corresponds well with experiment. Due to the neglegt of friction forces the Mach number level is calculated too high.

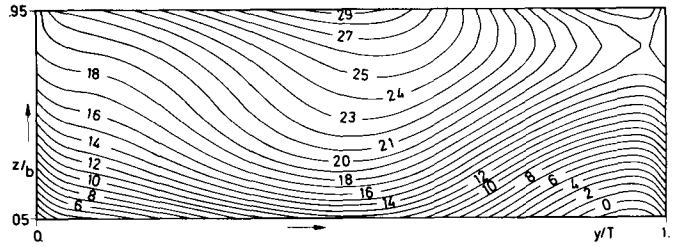

FIG. 9 Measured distribution of the absolute flow angles at λ = 1.1
n_{red} = 14,600 r.p.m.

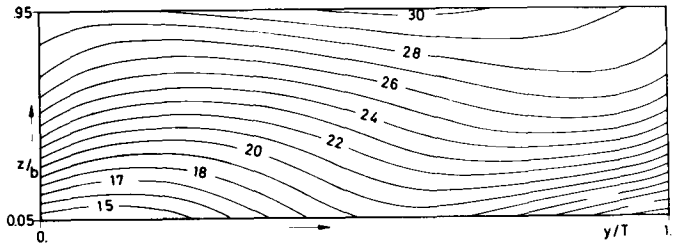

FIG.10 Predicted distribution of the absolute flow angles at λ = 1.1
n_{red} = 14,600 r.p.m.

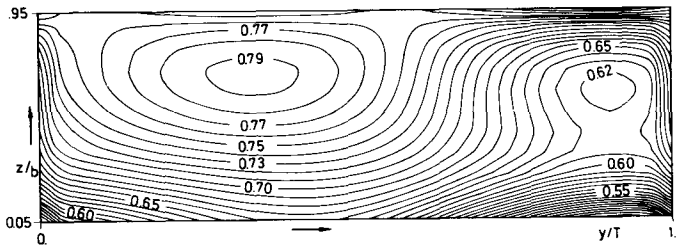

FIG.11 Measured distribution of the Mach numbers at λ = 1.1
n_{red} = 14,600 r.p.m.

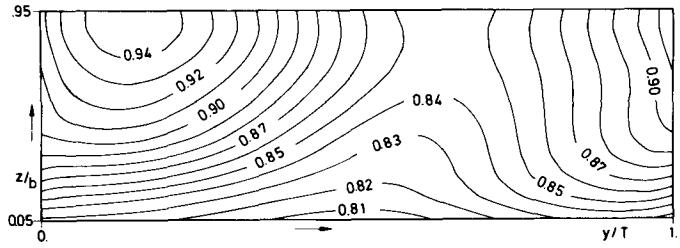

FIG.12 Predicted distribution of the Mach numbers at λ = 1.1
n_{red} = 14,600 r.p.m.

COMPARISON OF MEASURED AND PREDICTED PERFORMANCE MAPS

For practical purposes the evaluation of integral results of the considered unit is more essential than flowfield calculations. To characterize the diffuser efficiency a pressure recovery coefficient c_p defined by

$$c_P = \frac{\bar{p}_{DE} - \bar{p}_{IE}}{\bar{p}_t - \bar{p}_{IE}} \tag{8}$$

where $\bar{p}_{IE}$ and $\bar{p}_{DE}$ are average pressure values at the impeller and diffuser exit and $\bar{p}_t$ is the total pressure is plotted versus a nondimensional mass flux defined by

$$\dot{m}_D = \frac{1}{2\pi r_{IE} b \sqrt{p_t \varrho_t}} \int_0^b \int_0^{2\pi} r \cdot \varrho u_r \, d\Theta \, dz \tag{9}$$

A comparison of a predicted and measured performance map is shown in Fig. 13. For high-loaded machines the choking and suction line are determined by the vaned diffuser. Therefore the performance map of the diffuser gives interesting information about the operating range of the unit. It was found out previously that there exists a correlation between numerical and physical instabilities near the surge line [16].

As friction is neglected pressure recovery and maximum mass flux are estimated too large compared with measured data. One can improve the results of the inviscid theory by applying boundary layer theory along

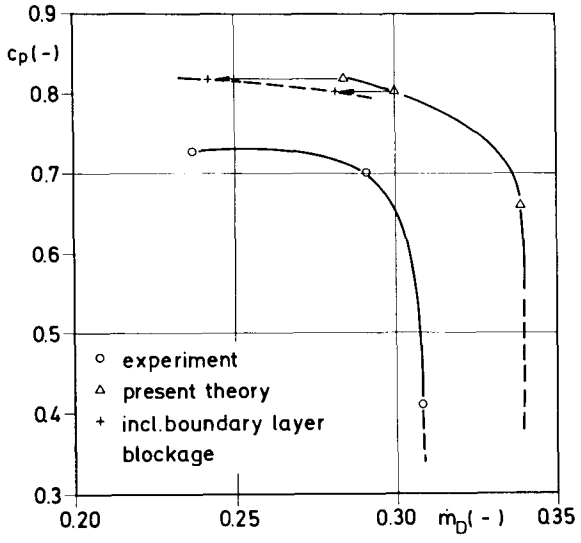

FIG.13 Measured and predicted performance map of Jansen's twisted diffuser

the intersecting lines between the blades and the S_1-stream surface as well as between the side walls and the S_2-stream surface. After calculating a blockage factor in the throat with the values of displacement thickness obtained by an entrainment method [17] one gets the results connected by a dotted line (Fig. 13). In spite of a better agreement there is yet a large defect left. As a consequence it has to be stated that a coupling of inviscid theory and boundary layer programs is not able to provide a better prediction of the phenomena in diffuser passages.

As the numerical integration of the complete or parabolized Navier-Stokes equations in connection with complex boundaries has remained a time-consuming process even if a vector computer is available one can improve the results by employing a simple loss model as e.g. given by Horlock [18]. However, the solution depends strongly on measured loss figures at special operating points and, therefore, one will only get reliable information about the loss mechanism in those cases, where experimental data are available.

CONCLUDING REMARKS

In this paper a method for calculating inviscid three-dimensional flowfields in vaned diffuser passages is described. For this purpose a quasi three-dimensional approach firstly given by Wu has been employed. The present procedure consisting of several FORTRAN programs has been applied for predicting the three-dimensional flow pattern in a diffuser with twisted vanes. A comparison of calculated and measured data shows good agreement. Also the diffuser performance map can be determined by the method within certain limits. The application of boundary layer theory, however, is not able to predict all the losses in the diffuser channel. Nevertheless, the described method provides valuable results for a better understanding of some important flow phenomena in radial diffusers.

REFERENCES

1 Kenny, D.P.: "Supersonic Radial Diffusers" in "Advanced Compressors", AGARD Lecture Series 39, 1970.

2 Japikse, D.: "Centrifugal Compressor Design", Concepts ETI, Course No. 2, 1981.

3 Jeske, H.O.; I. Teipel: "A Theoretical Investigation of Transonic Flows in Radial Compressor Diffusers", Journal of Engineering for Power, Vol. 105, pp.452-456, 1983.

4 Jansen, M.: "Untersuchung an beschaufelten Diffusoren eines hochbelasteten Radialverdichters", Ph. D. Thesis, Hannover 1982.

5 Wiedermann, A.: "Die raeumliche reibungslose Stroemung in Diffusoren eines Radialverdichters bei transsonischer Anstroemung", Ph. D. Thesis, Hannover 1985.

6 Wu, Ch.-H.: "A General Theory of Three-Dimensional Flow in Subsonic and Supersonic Turbomachines of Radial- ,Axial- and Mixed Flow Types", NACA TND 2604, 1952.

7 Marsh, H.: "A Digital Computer Program for the Through-flow Fluid Mechanics in an Arbitrary Turbomachine Using a Matrix Method", ARC R&M No. 3509, 1968.

8 Bosman, C.; M.A.I.El-Shaarawi: "Quasi-Three-Dimensional Numerical Solution of Flow in Turbomachines", Journal of Fluid Engineering, Vol. 99, pp.132-140, 1977.

9 Wilkinson, D.H.: "Calculation of Blade-to-Blade Flow in a Turbomachine by Streamline Curvature", ARC R&M No. 3704, 1972.

10 Novak, R.A.: "Streamline Curvature Computing Procedures for Fluid-Flow Problems", Journal of Engineering for Power, Vol.89, pp.478-490, 1967.

11 Krimerman, Y.; D.Adler: "The Complete Three-Dimensional Calculation of the Compressible Flowfield in Turbo Impellers", Journal Mechanical Engineering Science, Vol. 20 No. 3, pp.149-158, 1978.

12 Hirsch, Chr.;G. Warzee: "An Integrated Quasi-3D Finite Element Calculation Program for Turbomachinery Flows." ASME Paper No. 78-GT-56, 1978.

13 Wang, Q.; G.Zhu; Ch.-H.Wu: "Quasi-Three-Dimensional and Full Three-Dimensional Rotational Flow Calculations in Turbomachines", ASME Paper No. 84-GT-185, 1984.

14 MacCormack, R.W.: "The Effect of Viscosity in Hypervelocity Impact Cratering", AIAA-Paper 69-354, 1969.

15 Jansen, M.; M.Rautenberg: "Design and Investigations of a Three Dimensional Twisted Diffuser for a Centrifugal Compressor", ASME-Paper No. 82-GT-102, 1982.

16 Teipel, I.; A.Wiedermann: "The Influence of Different Geometries for a Vaned Diffuser on the Pressure Distribution in a Centrifugal Compressor", ASME-Paper No. 84-GT-68, 1984.

17 Green, J.E.; D.J.Weeks; J.W.F.Brooman: "Prediction of Turbulent Boundary Layers and Wakes in Compressible Flow by a Lag-Entrainment Method", ARC R&M No. 3791, 1973.

18 Horlock, J.H.: "On Entropy Production in Adiabatic Flow in Turbomachines", Journal of Basic Engineering ,Vol.93, pp. 587-593, 1971.